Experimental and Computational Study of Small (n = 1−16) Stoichiometric Zinc and Cadmium Chalcogenide Clusters

ARTICLE *in* THE JOURNAL OF PHYSICAL CHEMISTRY A · MARCH 2006

Impact Factor: 2.69 · DOI: 10.1021/jp056218v · Source: PubMed

3 AUTHORS, INCLUDING:

Andrei Burnin
Dartmouth College
12 PUBLICATIONS **186** CITATIONS

Experimental and Computational Study of Small ($n = 1-16$) Stoichiometric Zinc and Cadmium Chalcogenide Clusters

Edward Sanville, Andrei Burnin, and Joseph J. BelBruno*

Center for Nanomaterials Research and Department of Chemistry, Dartmouth College, Hanover, New Hampshire 03755

Received: October 28, 2005; In Final Form: December 17, 2005

Zinc selenide, cadmium sulfide, and cadmium selenide clusters were produced by direct laser ablation and analyzed in a time-of-flight mass spectrometer. The positive-ion mass spectra indicated that clusters composed of six and thirteen monomer units were ultrastable in all cases. The geometries and energies of the neutral and positively charged M_nX_n clusters up to $n = 16$ were obtained computationally at the B3LYP level of theory using the SKBJ basis set for the metal atoms and the SKBJ(*d*,2*df*) basis set for the chalcogen atoms. Small neutral and positive clusters ($n = 1-4$) have planar geometries, neutral three-dimensional clusters have the geometry of closed-cage polyhedra, and cationic three-dimensional clusters have structures with a pair of two-coordinated atoms. Physical properties of the clusters as a function of size are reported. The relative stability of the positive stoichiometric clusters provides a thermodynamic explanation for the relative stability observed experimentally from the laser-ablation mass spectrometry.

Introduction

The II−VI clusters represent an interesting focus of study. As semiconductors, the bulk materials are important wide band-gap materials, which can be used in the fabrication of opto-electronic devices such as blue or UV light-emitting diodes,[1] laser diodes, *n*-window layers in solar cell technology,[2] and emissive flat screens.[3] On the other hand, clusters represent the link between an ensemble of separate atoms or molecules and a bulk material. Some clusters exhibit exceptional stability relative to neighboring sizes. Those molecules are sometimes referred to as magic number clusters, whose exceptional stability may be conferred by either geometric or electronic considerations.

The chalcogenides and related clusters have been studied experimentally. The earliest study by Shi et al.[4] indicated preferential formation of $n = 13$ and 34 clusters by direct laser ablation of manganese sulfide. Martin[5] reported the distribution of ZnS clusters from a time-of-flight mass spectrometry study initiated by laser ablation of solid zinc sulfide followed by a helium gas quench of the vapor. Work in our group[6] using a different ablation/detection scheme confirmed the presence of ultrastable ZnS clusters of 13 and 33 or 34 monomer units. More recently, Kukreja et al.,[7] using similar techniques, confirmed the presence of these stable clusters for molecules of 6, 13, 19, 23, and 33 monomer units for ZnSe. The mass spectra of ZnO,[8] MnO,[9] and the sulfides of Fe and Cu,[4] neighbors of Zn ($d^{10}s^2$), Cd ($d^{10}s^2$), and Mn (d^5s^2) in the periodic table, did not indicate the formation of a significant excess of $n = 13$ clusters.

Theoretically, small neutral stoichiometric Zn_nS_n clusters ($n = 1-9$) were described using the density functional theory (DFT).[6,8,10,11] It was shown that Zn_2S_2 four-membered rings and Zn_3S_3 six-membered rings were the pertinent building blocks for larger three-dimensional structures. This idea was extended in a comparative theoretical study of the relative stability of hollow cage or bubble structures[12,13] versus bulklike crystallites for neutral clusters up to $n = 47$. Recent advances in structure prediction led to the use of a genetic algorithm[14] to predict the geometries of neutral clusters of up to fifteen monomer units. The Zn_nSe_n clusters were reported to prefer planar or near-planar rings when $n = 1-5$ and three-dimensional structures for clusters where $n = 6-9$, 12, or 15.[6,8,15] Similar observations have been reported for neutral Cd_nS_n and Cd_nSe_n clusters.[16] Other computational studies had previously examined the CdS and CdSe clusters at varying (lower) levels of theory and concluded, most likely as a result of the theory level, that alternative structures were the lowest-energy conformers.[17,18]

Almost all of the work cited has focused on the neutral clusters. In the single exception, a study that explored the $Zn_nS_n^+$ clusters, it was shown that the cations prefer different geometries from the neutral clusters.[11] The zinc and cadmium chalcogenide systems remain not fully understood with respect to the relative stability of the clusters, as revealed from time-of-flight mass spectrometry (TOF-MS) experiments. In fact, the source of the mass spectrum, cationic or neutral clusters, remains in doubt. Here, we focus on the relationship of the cluster structures to their physical properties and to the laser-ablation mass spectrum with a special emphasis on the cationic clusters. We demonstrate the similarity (and several differences) among the geometries of the target cationic clusters and the correspondence of the experimental mass spectrum to the relative ion cluster stability by DFT calculations.

Experimental Details

Metal chalcogenide clusters were generated in a time-of-flight mass spectrometer equipped with a Nd:YAG laser as described previously[11] using the fundamental (1064 nm) and/or second harmonic (532 nm) of a Nd:YAG laser (Spectra Physics DCR-3). The ablation process was carried out with a 500-cm focal-length quartz lens. So equipped, the laser provided fluences in the range from 0.2 to 4.5 J cm^{-2} in a 10 ns pulse. The materials used for cluster production included 99.99% pure zinc selenide powder, 99.999% pure cadmium sulfide powder, and 99.999% pure cadmium selenide powder (Strem Chemicals). Whereas some spectra were recorded using a pulsed valve with helium

10.1021/jp056218v CCC: $33.50
Published on Web 02/02/2006

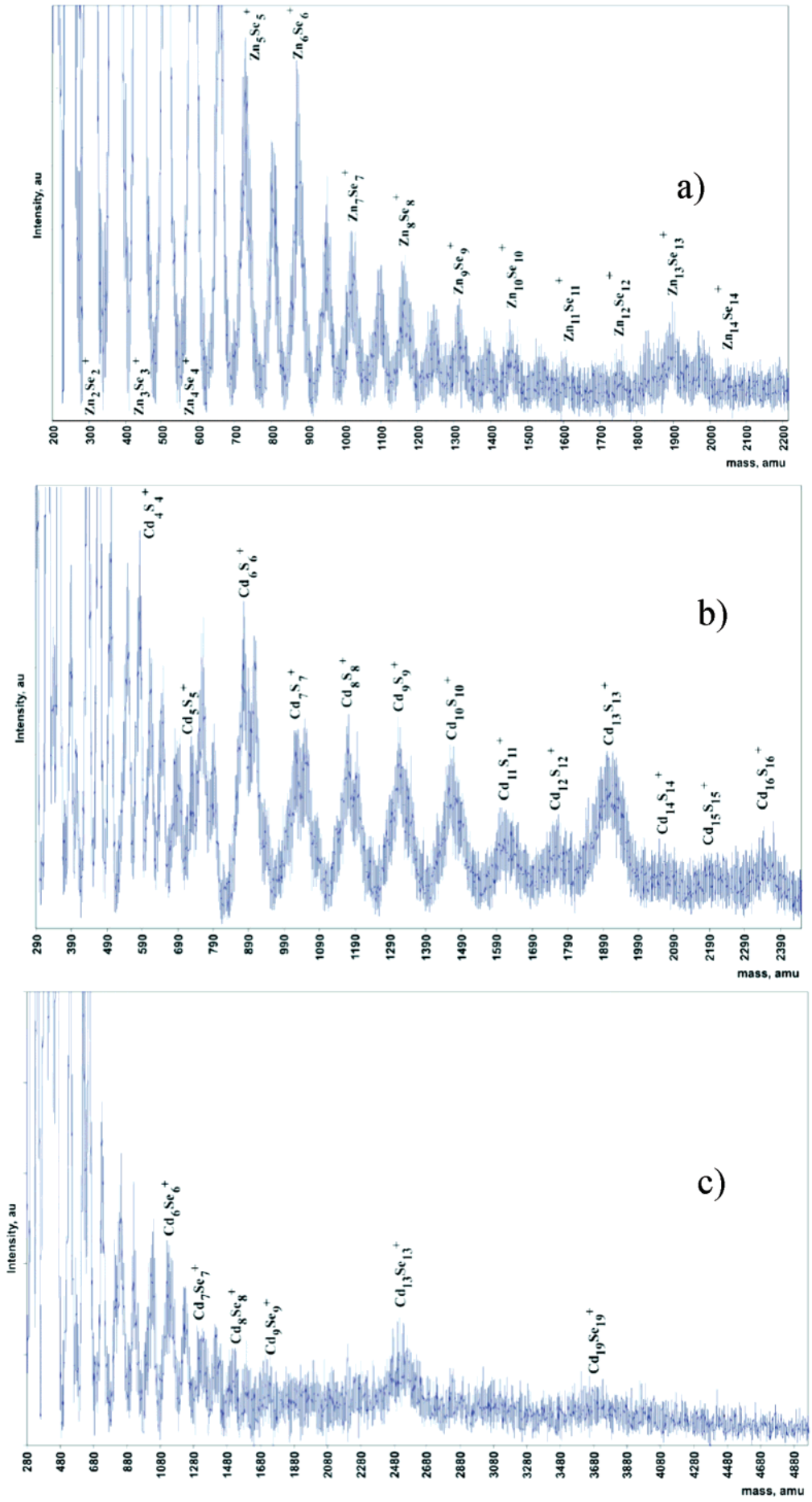

Figure 1. Mass spectra of (a) Zn_nSe_n, (b) Cd_nS_n, and (c) Cd_nSe_n clusters obtained by laser ablation.

buffer gas, those reported here were obtained in a vacuum (5×10^{-6} Torr). The positive ions were extracted, after a variable delay typically set to 60 μs, by a 99 V pulse, creating a field of 22.5 V/cm and immediately accelerated to 750 eV into a field-free flight tube of 2.28 m length. The clusters are separated in the flight tube, and the TOF signals are detected by a channeltron electron multiplier (Galileo Electrooptics), accumulated over 1000 traces in a digital oscilloscope and processed in a PC.

Computational Details

Geometric and topological trends for small stoichiometric Zn_nS_n clusters have been established previously by our group and others.[8,10,11] Topologically equivalent Zn_nSe_n, Cd_nS_n, and Cd_nSe_n structures corresponding to the previously located Zn_nS_n global minima were used as starting geometries for neutral and positive cluster optimizations in this study. The number of electrons in these clusters makes high level ab initio or DFT structural optimization calculations very CPU intensive. By necessity, we have limited the computational method to effective core potentials so that metal atom electrons unrelated to the bonding may be treated more easily. All optimizations, in the absence of any constraints, were performed using the Kohn−Sham hybrid density functional method[19,20] with *NWChem, Version 4.6*.[21] The correlation and exchange effects were calculated at the B3LYP level of theory[22] with the SKBJ basis set[23] for zinc and cadmium atoms. The expanded SKBJ(*d*,2*df*) basis set with the additional *d* and *f* functions of Matxain et al.[16] was used for sulfur and selenium atoms. In addition to the full optimizations, single-point calculations at the same level of theory were performed on positively charged clusters with the optimized geometries of the neutral clusters in order to find the vertical ionization energies. All calculations were run using the Dartmouth GreenGrid array of IBM eServer 325 machines, each containing dual 64-bit AMD Opteron processors equipped with 2 GB of RAM.

Results and Discussion

Mass Spectra. Mass spectra of ZnS have been previously reported.[6,11] The mass spectra obtained by laser ablation of solid ZnSe, CdS, and CdSe are shown in Figure 1. With two exceptions, the peak intensities fit a log-normal distribution and decrease quickly as a function of the number of monomer units. In each experimental spectrum, the signals correspond to the masses of three different classes of clusters: $M_nX_n^+$, $M_nX_{n+1}^+$, and $M_{n+1}X_n^+$. Peak broadening is caused by the overlap of unresolved signals from cluster isotopomers composed of the following major isotopes (with percent abundances): ^{64}Zn (48.63), ^{66}Zn (27.90), ^{67}Zn (4.10), ^{68}Zn (18.75); ^{76}Se (9.37), ^{77}Se (7.63), ^{78}Se (23.77), ^{80}Se (49.61), ^{82}Se (8.72); ^{32}S (94.93), ^{34}S (4.29); ^{106}Cd (1.25), ^{110}Cd (12.49), ^{111}Cd (12.8), ^{112}Cd (24.13), ^{113}Cd (12.22), ^{114}Cd (28.73), and ^{116}Cd (7.49).[24]

Neutral Clusters. It has been established by Ugalde and co-workers[10] and our group[11] that d^{10} metal chalcogenide clusters prefer bonding topologies in which only heteronuclear bonds are present. In fact, this is the most important driving force behind the global minimum geometries of these clusters, and therefore, only structures with heteronuclear bonding configurations were used in this study. The optimized geometries of these clusters are shown in Figure 2, and geometric parameters are summarized in Tables 1−3. We find that the small, neutral M_nX_n clusters ($n < 6$), have optimized geometries composed of two-coordinated atoms only. All of these two-coordinated geometries were found to be planar with the exception of M_5X_5, which adopted a slightly distorted envelope structure, similar to that

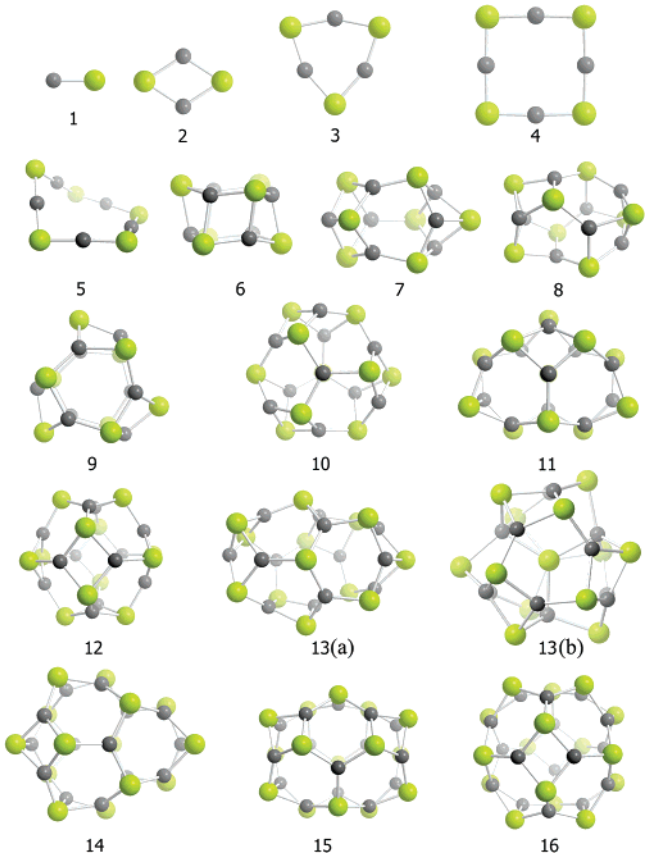

Figure 2. Geometric structures of the global minima neutral M_nX_n clusters with $n = 1-16$. Here, dark spheres are metal atoms and light spheres are chalcogen atoms.

previously reported for Zn_5S_5.[8,10,11] All of the neutral clusters with $n = 6-16$ take on closed polyhedron geometries composed of four- and six-membered rings. As previously described,[11] Euler's Theorem indicates that, for such structures, the total number of four-membered rings is a constant, $N_4 = 6$, whereas the number of six-membered rings is given by $N_6 = n - 4$, where n is the total number of monomer units. With several exceptions, our calculated geometries for the neutral clusters of up to nine monomer units agree with those reported by Matxain et al.[8,10] These are the only quantitative data available in the literature for comparison. Because the main points regarding the geometries of many of the neutral clusters have already been reported, only deviations from the previously reported structures and issues relevant to our subsequent discussion are presented. However, all of the structures are shown in the figure. Many of the deviations from the symmetry of a previously reported structure are small and may reflect the presence of low-frequency vibrational modes in these clusters.

The *1-mer* clusters have $C_{\infty v}$ symmetry. With the exception of ZnSe, the bond lengths in our calculations are in agreement with those previously reported.[16,25] In the case of ZnSe, we located a global minimum with a bond length of 2.295 Å. We find that the neutral *4-mer* clusters exhibit cyclic planar geometries with D_{4h} symmetry. In contrast, the previous study[8] reported a nonplanar C_{2v} geometry with similar bond lengths and bond angles. Steric repulsion between zinc atoms is negligible, but steric repulsion between opposite cadmium atoms causes the cluster to distort from a perfectly square geometry, causing the metal atom angles to deviate from 180°, while retaining D_{4h} symmetry. Because of the small size of the sulfur atom relative to the selenium atom and subsequent smaller ring size, steric repulsion causes more severe distortion to the Cd_4S_4

TABLE 1: Symmetry Point Groups, Bond Length Ranges, Bond Angle Ranges, and Vertical Ionization Energies of Zn_nSe_n and $Zn_nSe_n^+$ ($n = 1-16$) Clusters

structure	symmetry	R(M−X), Å	<(M−X−M), deg	<(X−M−X), deg	vertical IE, eV
ZnSe	$C_{\infty v}$	2.295	−	−	8.34
$ZnSe^+$		2.299			
Zn_2Se_2	D_{2h}	2.380	63.1	116.9	8.11
$Zn_2Se_2^+$		2.390	66.2	113.8	
Zn_3Se_3	D_{3h}	2.320	79.6	160.4	8.39
$Zn_3Se_3^+$	C_{2v}	2.303−2.392	81.7−82.3	157.9−158.0	
Zn_4Se_4	D_{4h}	2.302	90.0	180.0	8.05
$Zn_4Se_4^+$		2.307	92.1	177.9	
Zn_5Se_5	C_1	2.296−2.301	89.9−96.1	173.2−178.5	8.11
$Zn_5Se_5^+$		2.289−2.322	91.8−98.9	173.7−179.2	
Zn_6Se_6	D_{3d}	2.426−2.584	71.0−92.4	103.5−140.8	7.97
$Zn_6Se_6^+$	C_s	2.322−2.566	70.9−97.1	102.1−156.2	
Zn_7Se_7	C_{3v}	2.415−2.494	68.8−99.1	101.9−132.5	8.00
$Zn_7Se_7^+$	C_2	2.303−2.585	67.7−101.9	97.6−157.6	
Zn_8Se_8	S_4	2.406−2.543	70.0−102.1	101.9−138.2	7.89
$Zn_8Se_8^+$	C_1	2.298−2.602	68.3−107.4	100.6−161.6	
Zn_9Se_9	C_{3h}	2.400−2.508	72.2−100.4	101.7−139.5	7.89
$Zn_9Se_9^+$	C_1	2.300−2.554	70.3−103.1	97.6−159.4	
$Zn_{10}Se_{10}$	C_3	2.386-2.517	69.7−103.3	99.2−138.2	7.73
$Zn_{10}Se_{10}^+$	C_s	2.295−2.544	69.2−102.7	96.9−160.5	
$Zn_{11}Se_{11}$	C_s	2.389−2.510	71.5−104.2	95.5−138.9	7.77
$Zn_{11}Se_{11}^+$	C_1	2.292−2.560	68.5−105.9	95.8−160.0	
$Zn_{12}Se_{12}$	O_h	2.389−2.475	74.8−99.5	98.9−130.2	7.93
$Zn_{12}Se_{12}^+$	C_s	2.362−2.481	72.8−100.5	93.0−132.9	
$Zn_{13}Se_{13}$ (a)	C_1	2.385−2.511	70.7−107.7	96.4−138.2	7.75
$Zn_{13}Se_{13}$ (b)	C_3	2.309−2.675	72.7−115.7	97.1−161.0	7.69
$Zn_{13}Se_{13}^+$ (a)	C_2	2.206−2.402	77.3−114.6	97.6−161.5	
$Zn_{13}Se_{13}^+$ (b)	C_1	2.310−2.787	80.6−163.3	73.0−121.7	
$Zn_{14}Se_{14}$	C_s	2.383−2.519	71.1−106.6	96.6−137.3	7.79
$Zn_{14}Se_{14}^+$	C_1	2.311−2.504	72.6−107.8	95.5−164.0	
$Zn_{15}Se_{15}$	C_{3h}	2.385−2.476	74.4−105.8	98.9−131.5	7.75
$Zn_{15}Se_{15}^+$	C_s	2.353−2.544	73.7−107.1	93.8−137.9	
$Zn_{16}Se_{16}$	T_d	2.418−2.456	75.0−103.1	98.4−130.6	7.74
$Zn_{16}Se_{16}^+$	C_{2v}	2.369−2.514	74.9−105.7	86.2−136.5	

ring than to the Cd_4Se_4 ring. We observed that the neutral *5-mer* clusters are the smallest clusters with predicted nonplanar geometry. They have a distorted envelope structure with C_1 symmetry, similar to what we previously found[11] for Zn_5S_5. It is clear that the M_5X_5 ring is large enough so that steric repulsion between metal atoms is no longer of great importance. Rather, the important factor in determining chalcogen bond angles here is the preference of the selenium atoms for unhybridized 90° *p*-orbital bonding. This is the first cluster sufficiently large to allow this preference to be exhibited. The M−X−X−M dihedral angles were 23.6, 16.8, and 21.3° for ZnSe, CdS, and CdSe, respectively, confirming that this is the cause of the ring distortion. The structures of subsequent clusters reflect competition between the preference for the 90° bond angle and the driving force for three-coordinate bonding. Previous studies[25] located a C_s minimum for the pentamer with similar geometric parameters.

Our calculations indicate that the neutral *7-mer* clusters take on an Euler closed-cage structure composed of 3 six-membered rings and 6 four-membered rings. There are 2 opposite sets of 3 adjacent four-membered rings, each with 3 strained 4−4 bonds. This structure has C_{3v} symmetry and differs from the previously reported[25] lower-symmetry C_s geometry. The neutral *10-mer* cluster geometry is a closed-cage structure composed of 6 six-membered rings. There are 3 sets of 2 adjacent four-membered rings, each resulting in a strained 4−4 bond. This structure has C_3 symmetry in agreement with the reported structures for the cadmium chalcogenides; there are no previous results for $Zn_{10}Se_{10}$ (nor for the Zn_nSe_n, $n = 11$, 13, 14, and 16 clusters). The neutral *11-mer* clusters are also closed-cage structures composed of 7 six-membered rings. There are 2 sets of 2 adjacent four-membered rings in this structure and a total of 2 strained 4−4 bonds. The structure has C_s symmetry. The optimized parameters for the *12-mer* clusters are in agreement[16] with previous work. These are closed-cage structures composed of 8 six-membered rings. All 6 of the four-membered rings within the structure are separated, resulting in no strained 4−4 bonds and additional structural stability. We find that the structure has O_h symmetry for $Zn_{12}Se_{12}$ and $Cd_{12}Se_{12}$ and C_i symmetry for $Cd_{12}S_{12}$, rather than the previously reported[8] D_{2h}. For each pair of elements, two different geometries for the neutral *13-mer* structures were investigated. The first geometry, (a), is a closed-cage structure composed of 9 six-membered rings. There are two pairs of adjacent four-membered rings within this structure of C_1 symmetry, resulting in two strained 4−4 bonds. The second geometry, (b), is a distorted nanocrystalline structure, previously reported for $Cd_{13}Se_{13}$.[15] This structure contains a single four-coordinate metal atom and a single four-coordinate chalcogen atom. Within the external cage, all but three metal atoms are three-coordinate; the three exceptional metal atoms are only two-coordinate. The structure has C_3 symmetry. This core-cage structure is the global minimum geometry for both $Cd_{13}S_{13}$ and $Cd_{13}Se_{13}$, but only a local minimum for $Zn_{13}S_{13}$ and $Zn_{13}Se_{13}$. Cadmium tends to stabilize nanocrystalline nanoclusters with four-coordinate atoms, relative to zinc. The neutral *14-mer* clusters adopted a closed-cage structure identical that reported for the cadmium chalcogenides, composed of 10 six-membered rings. The structure has a single pair of adjacent four-membered rings, one strained 4−4 bond and C_s symmetry. Finally, the *16-mer* clusters adopted a closed-cage structure composed of 12 six-membered rings, without adjacent four-membered rings, again in agreement with the corresponding cadmium clusters. The structure has T_d symmetry.

TABLE 2: Symmetry Point Groups, Bond Length Ranges, Bond Angle Ranges, and Vertical Ionization Energies of Cd_nS_n and $Cd_nS_n^+$ ($n = 1-16$) Clusters

structure	symmetry	R(M−X), Å	<(M−X−M), deg	<(X−M−X), deg	vertical IE, eV
CdS	$C_{\infty v}$	2.295	−	−	8.24
CdS^+		2.388			
Cd_2S_2	D_{2h}	2.490	69.2	110.8	8.10
$Cd_2S_2^+$		2.500	73.4	106.6	
Cd_3S_3	D_{3h}	2.416	84.1	155.9	8.45
$Cd_3S_3^+$	C_{2v}	2.397−2.491	87.0−87.7	152.2−153.8	
Cd_4S_4	D_{4h}	2.390	94.0	175.9	8.17
$Cd_4S_4^+$		2.395	96.8	173.2	
$Cd_5S_5^+$	C_1	2.383−2.385	97.6−101.0	175.4−179.8	8.27
Cd_5S_5		2.372−2.408	100.5−104.3	176.7−179.9	
Cd_6S_6	D_{3d}	2.506−2.746	76.9−95.6	98.4−143.2	8.02
$Cd_6S_6^+$	C_s	2.417−2.713	77.0−102.6	96.9−150.3	
Cd_7S_7	C_{3v}	2.505−2.594	74.8−101.9	98.4−129.5	8.00
$Cd_7S_7^+$	C_2	2.397−2.707	74.0−106.4	94.2−151.8	
Cd_8S_8	S_4	2.492−2.682	76.0−105.0	96.8−138.7	7.94
$Cd_8S_8^+$	C_1	2.389−2.720	74.4−111.7	96.8−156.1	
Cd_9S_9	C_{3h}	2.489−2.623	78.2−103.1	97.5−139.0	7.94
$Cd_9S_9^+$	C_1	2.389−2.657	76.3−107.5	93.7−154.0	
$Cd_{10}S_{10}$	C_3	2.474−2.637	75.8−105.9	95.3−137.7	7.90
$Cd_{10}S_{10}^+$	C_s	2.460−2.712	70.5−105.0	92.6−168.6	
$Cd_{11}S_{11}$	C_s	2.475−2.637	77.4−108.0	91.5−138.7	7.95
$Cd_{11}S_{11}^+$	C_1	2.384−2.665	74.5−110.9	92.0−154.4	
$Cd_{12}S_{12}$	C_i	2.473−2.580	80.7−102.8	94.2−131.6	8.09
$Cd_{12}S_{12}^+$	C_s	2.413−2.616	79.8−106.4	83.2−137.1	
$Cd_{13}S_{13}$ (a)	C_1	2.475−2.640	76.6−112.2	93.0−137.9	7.83
$Cd_{13}S_{13}$ (b)	C_3	2.402−2.784	78.6−117.6	93.1−155.8	7.78
$Cd_{13}S_{13}^+$(a)	C_2	2.414−2.635	81.0−119.8	94.6−161.8	
$Cd_{13}S_{13}^+$(b)	C_1	2.407−2.895	79.1−127.7	76.5−159.1	
$Cd_{14}S_{14}$	C_s	2.468−2.648	77.0−109.5	92.2−136.4	7.87
$Cd_{14}S_{14}^+$	C_1	2.401−2.608	79.3−116.7	92.2−159.8	
$Cd_{15}S_{15}$	C_{3h}	2.471−2.582	80.4−110.3	94.4−132.3	7.94
$Cd_{15}S_{15}^+$	C_s	2.468−2.648	77.0−109.5	92.2−136.4	
$Cd_{16}S_{16}$	T_d	2.512−2.552	81.2−107.1	94.7−131.5	7.91
$Cd_{16}S_{16}^+$	C_{2v}	2.571−2.614	77.6−105.9	97.4−130.5	

Positively Charged Clusters. The positively charged metal chalcogenide clusters have not been previously reported. The optimized geometries of the global minimum cationic clusters ($n = 1-16$) are shown in Figure 3, and summarized in Tables 1−3. In the figure, clusters are labeled according to the number of monomer units. Geometrically, the small, positive d^{10} metal chalcogenide clusters ($n < 6$) retained the connectivity of their neutral counterparts. All of the large, three-dimensional positive clusters ($n > 5$) contained a pair of two-coordinate atoms, with the exception of the 12-, 15-, and 16-mers. The two-coordinate atoms appear to improve the structural energy by eliminating pairs of adjacent four-membered rings, reducing the number of strained 4−4 bonds. This also reduces N_4 from six to four, while increasing N_6 by one to $n - 3$ in each case. Significantly, in the case of the 12-, 15-, and 16-mers, the neutral geometry contains no adjacent four-membered rings, and therefore formation of two-coordinate atoms is energetically unfavorable. Bond lengths and bond angles, of course, may take on different values from those in the neutral clusters, but the variation was small. It is not possible to further generalize the magnitude or direction of these changes with ion formation from the neutrals.

The positive *1-mer* clusters are, of course, linear with $C_{\infty v}$ symmetry. The bond lengths are slightly shorter than those in the corresponding neutral monomer. The *2-mer* cationic clusters retained diamond-shaped planar geometries with D_{2h} symmetry. The bond lengths were essentially unchanged from the neutrals, but the M−X−M bond angles were larger in the positive planar structures, possibly due to increased metal−metal Coulombic repulsion caused by additional positive charge density on these atoms. The *3-mer* clusters, with slight distortion, retained shield-like planar geometries. The distortion caused symmetry-lowering and resulted in C_{2v} symmetry. The distortion is a result of the removal of a single electron from the doubly degenerate HOMO of the neutral trimer. The bond lengths bracketed the neutral bond lengths and M−X−M bond angles were identical to the neutrals. The cationic *4-mer* clusters have planar geometries with D_{4h} symmetry. Metal chalcogenide bond lengths and bond angles were essentially identical those of the neutral clusters. The positive *5-mer* clusters retained a distorted envelope structure with C_1 symmetry, as in the neutral clusters. Bond length and angle ranges were broader than in the neutrals. The M−X−X−M dihedral angles were reduced from those of the neutral clusters, 19.0, 13.4, and 16.9° (for ZnSe, CdS, and CdSe), indicating a greater planarity than in the neutral clusters.

Bond length ranges increased for the clusters with $n > 5$. This is in concert with a general decrease in the symmetry of the cationic clusters in comparison to the neutrals in this size range. The *6-mer* cluster cations begin the sequence of three-dimensional structures. These clusters adopted a hexagonal prism geometry with an opened metal−chalcogen bond, eliminating a strained 4−4 bond. This structure has C_s symmetry, indicating distortion from the more symmetric D_{3d} neutral cluster. Bond length and angle ranges were broader. The positive *7-mer* cluster structure contains two pairs of adjacent four-membered rings, and 2 two-coordinated atoms. This structure has C_2 symmetry as opposed to the C_{3v} symmetry of the corresponding neutral cluster. The distortion from the neutral geometry is evident from the extended bond-length range. The cationic *8-mer* clusters take on a structure containing two pairs of adjacent four-membered rings and 2 two-coordinated atoms. This structure has C_1 symmetry, not the high S_4 symmetry of the neutral cluster. Bond lengths are longer than in the corresponding neutral. The M−X−M bond angle ranges are also correspondingly greater. The positive *9-mer* cluster structure

TABLE 3: Symmetry Point Groups, Bond Length Ranges, Bond Angle Ranges, and Vertical Ionization Energies of Cd_nSe_n and $Cd_nSe_n^+$ ($n = 1-16$) Clusters

structure	symmetry	R(M−X), Å	<(M−X−M), deg	<(X−M−X), deg	vertical IE, eV
CdSe	$C_{\infty v}$	2.404	−	−	7.98
$CdSe^+$		2.495			
Cd_2Se_2	D_{2h}	2.595	66.8	113.2	7.82
$Cd_2Se_2^+$		2.583	78.0	102.0	
Cd_3Se_3	D_{3h}	2.523	81.6	158.4	8.09
$Cd_3Se_3^+$	C_{2v}	2.496−2.565	84.3−84.4	155.4−155.8	
Cd_4Se_4	D_{4h}	2.499	91.6	178.3	7.78
$Cd_4Se_4^+$		2.503	93.9	176.1	
Cd_5Se_5	C_1	2.492−2.497	92.9−98.0	174.0−178.9	7.80
$Cd_5Se_5^+$		2.484−2.518	95.3−101.0	175.0−179.7	
Cd_6Se_6	D_{3d}	2.618−2.849	74.3−93.2	100.1−144.2	7.66
$Cd_6Se_6^+$	C_s	2.523−2.819	74.2−99.2	98.9−153.9	
Cd_7Se_7	C_{3v}	2.617−2.708	72.1−99.5	99.7−132.2	7.67
$Cd_7Se_7^+$	C_2	2.503−2.816	71.2−103.2	95.3−155.3	
Cd_8Se_8	S_4	2.604−2.787	73.4−102.3	98.6−140.0	7.58
$Cd_8Se_8^+$	C_1	2.495−2.835	71.7−108.2	98.1−159.6	
Cd_9Se_9	C_{3h}	2.598−2.730	75.4−100.8	99.2−140.9	7.58
$Cd_9Se_9^+$	C_1	2.497−2.772	73.4−103.6	94.8−157.5	
$Cd_{10}Se_{10}$	C_3	2.584−2.745	73.1−103.1	96.5−139.6	7.49
$Cd_{10}Se_{10}^+$	C_s	2.491−2.760	72.4−104.9	93.8−158.5	
$Cd_{11}Se_{11}$	C_s	2.584−2.746	74.7−105.0	92.5−140.5	7.60
$Cd_{11}Se_{11}^+$	C_1	2.490−2.777	71.8−106.9	92.9−157.8	
$Cd_{12}Se_{12}$	O_h	2.532−2.667	76.4−104.3	96.2−132.5	8.21
$Cd_{12}Se_{12}^+$	D_{2h}	2.557−2.692	76.5−101.4	90.3−133.8	
$Cd_{13}Se_{13}$ (a)	C_1	2.584−2.747	73.9−108.8	93.8−139.6	7.45
$Cd_{13}Se_{13}$ (b)	C_3	2.509−2.894	75.7−116.6	95.4−159.4	7.42
$Cd_{13}Se_{13}^+$(a)	C_2	2.605−2.796	79.7−121.9	96.0−164.2	
$Cd_{13}Se_{13}^+$(b)	C_1	2.512−2.974	76.3−126.3	77.7−163.2	
$Cd_{14}Se_{14}$	C_s	2.578−2.754	74.2−106.3	93.4−138.3	7.48
$Cd_{14}Se_{14}^+$	C_1	2.507−2.718	76.2−110.9	93.0−162.5	
$Cd_{15}Se_{15}$	C_{3h}	2.580−2.692	77.5−106.8	95.9−132.5	7.51
$Cd_{15}Se_{15}^+$	C_s	2.548−2.726	76.9−109.1	90.2−138.4	
$Cd_{16}Se_{16}$	T_d	2.622−2.664	78.3−103.9	96.0−131.6	7.49
$Cd_{16}Se_{16}^+$	C_{2v}	2.565−2.743	78.4−107.9	82.6−138.1	

contains one pair of adjacent four-membered rings, and 2 two-coordinated atoms. This structure has reduced symmetry, C_1, in comparison to the neutral molecule C_{3h} symmetry.

The positive *10-mer* and *11-mer* clusters adopted structures with no adjacent four-membered rings and 2 two-coordinated atoms. The cationic *10-mer* has C_s symmetry, whereas the neutral cluster exhibited C_3 symmetry. The ion structure with 11 atoms has C_1 symmetry instead of the C_s symmetry of the corresponding neutral cluster. The positive *12-mer* clusters adopted the closed-cage Euler topology of the neutral 12-mer clusters but with slightly lower symmetries. The $Zn_{12}Se_{12}^+$ and $Cd_{12}S_{12}^+$ clusters adopted C_s symmetry, whereas the $Cd_{12}Se_{12}^+$ cluster adopted D_{4h} symmetry. All 3 positive *12-mer* clusters also have greater ranges of geometry parameters.

Two different geometries for the *13-mer* structures were investigated. The first geometry, **a**, is a structure containing 4 nonadjacent four-membered rings and 2 two-coordinated atoms. This structure has C_2 symmetry and was the global minimum structure for all 3 ions. The second structure, **b**, relaxed to a distorted nanocrystalline structure similar to $M_{13}X_{13}$ **b**, with the four-coordinate chalcogen atom moved slightly from the primary C_3 axis. This results in C_1 symmetry. The C_1 symmetry-positive *14-mer* cluster structure has 4 nonadjacent four-membered rings and 2 two-coordinate atoms. The cations returned to highly symmetric structures as additional monomer units are added. The positive *15-mer* clusters adopted a closed-cage Euler topology of C_s symmetry, slightly distorted from the C_{3h} neutral $M_{15}X_{15}$ clusters and the positive *16-mer* clusters retained the closed-cage Euler topology of the neutral $M_{16}X_{16}$ clusters. However, all of the positive *16-mer* clusters adopted a lower symmetry of C_{2v}.

Cluster Properties. The relative stability of stoichiometric clusters is generally rationalized in terms of the *incremental atomization energy*, $\Delta E_{at}(M_nX_n)$,

$$\Delta E_{at}(M_nX_n) = E_{M_{n-1}X_{n-1}} + E_M + E_X - E_{M_nX_n} \qquad (1)$$

where E_Y is the total electronic energy of species Y. Greater incremental atomization energies, therefore, imply greater stability relative to the next-smaller cluster size. Graphs of the incremental atomization energies of M_nX_n with respect to n are shown in Figure 4. The data for the Zn−S system are taken from previous calculations by our group[11] at the higher B3LYP/6-311+G* level of theory. There is remarkable similarity in the computed pattern of incremental atomization energies for the neutral clusters across all four metal chalcogenide combinations. However, the qualitative results in the figure are not consistent with the experimental cluster intensities. This will be addressed below. The patterns of incremental atomization energies for the neutral three-dimensional clusters can be understood in terms of energy stabilization for relieving bond strain by separating a pair of adjacent four-membered rings. For each pair of four-membered rings that is separated, a highly strained 4−4 bond connecting two adjacent four-membered rings is eliminated, resulting in an additional stabilization to the cluster of 0.34−0.40 eV. The ability of a structure to eliminate strain in this way is dictated by the geometric structure of the cluster and, hence, the exact number of monomer units that make up the cluster. This leads to a similar energetic pattern for all sets of neutral d^{10} metal chalcogenide clusters in the calculations. In the case of the closed Euler polyhedron neutral clusters, a simple model can be used to predict the incremental atomization

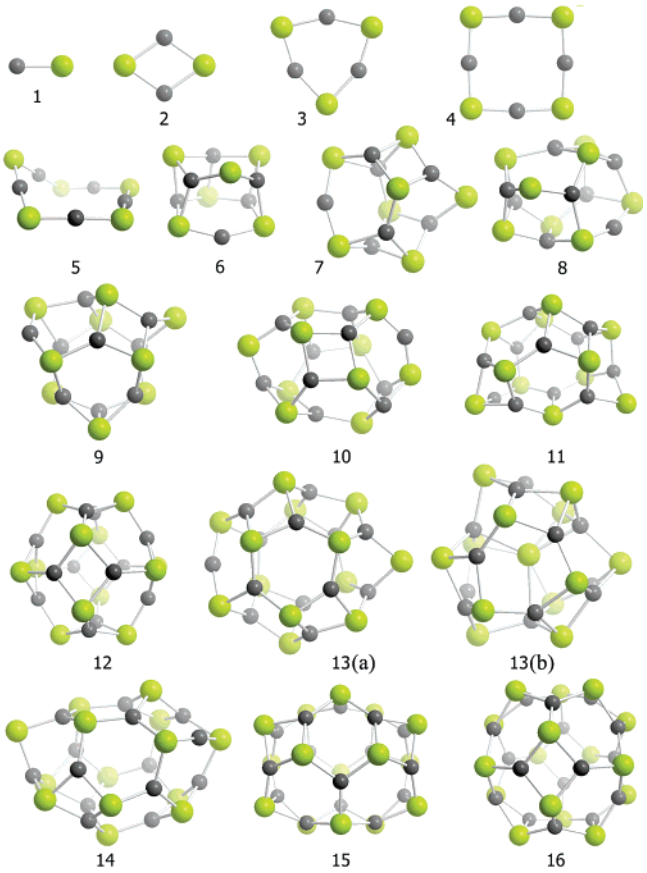

Figure 3. Geometric structures for the global minima $M_nX_n^+$ clusters with $n = 1-16$. Dark spheres represent metal atoms and light spheres are chalcogen atoms.

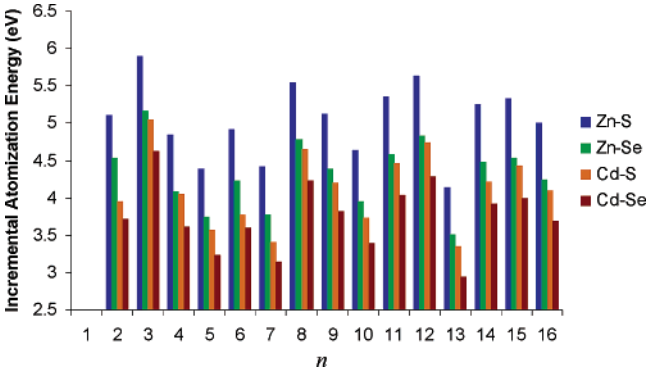

Figure 4. Incremental atomization energies of M_nX_n, clusters in electronvolts, with respect to n for Zn_nS_n, Zn_nSe_n, Cd_nS_n, and Cd_nSe_n.

energies of the clusters with fairly good precision:

$$\Delta E_{at}(M_nX_n) = [b_{4-4}(M_{n-1}X_{n-1}) - b_{4-4}(M_mX_m)]\Delta E_{4-4} + \Delta E_{mon} \quad (2)$$

where $\Delta E_{at}(M_nX_n)$ is the incremental atomization energy of the neutral n-mer, $b_{4-4}(M_mX_m)$ is the number of 4−4 bonds present in the m-mer, ΔE_{4-4} is the destabilization energy per 4−4 bond, and ΔE_{mon} is the incremental atomization energy of a cluster in the absence of 4−4 bond formation or elimination. The patterns of incremental atomization energies for each of the metal chalcogenide combinations were fit by varying the two parameters ΔE_{4-4} and ΔE_{mon}. The model prediction is compared with the calculated incremental atomization energies of zinc sulfide clusters in Figure 5. The calculated parameters for each metal chalcogenide combination are shown in Table 4.

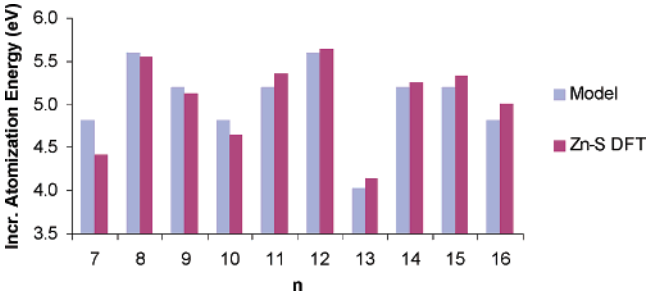

Figure 5. Incremental atomization energies of Zn_nS_n clusters calculated with DFT, compared with the predicted pattern using the 4−4 bond-strain model, with respect to n.

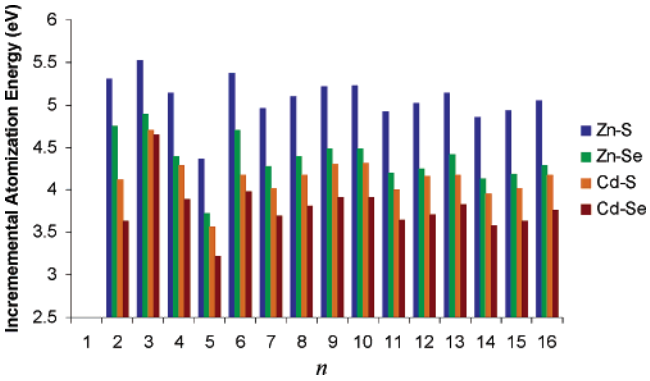

Figure 6. Incremental atomization energies of $M_nX_n^+$ clusters, in electronvolts, with respect to n for $Zn_nS_n^+$, $Zn_nSe_n^+$, $Cd_nS_n^+$, and $Cd_nSe_n^+$.

TABLE 4: Fitted Values of the Parameters ΔE_{4-4} and ΔE_{mon} for Each Metal Chalcogenide Combination, Using the 4−4 Bond Strain Model (eq 2)

M−X	ΔE_{4-4}, eV	ΔE_{mon}, eV
Zn−S	0.394	4.810
Zn−Se	0.350	4.098
Cd−S	0.374	3.904
Cd−Se	0.359	3.530

The question of the formation mechanism of the ions in the experimental mass spectra is qualitatively focused on whether neutral clusters are formed in the ablation process and then ionized from that initial distribution or whether the ions are formed directly in the ablation process itself. In our work with ZnS clusters, it was found that the incremental atomization energies of the positive clusters were correlated with the experimental TOF spectra. Calculated incremental atomization energies for the cation clusters are presented in Figure 6. In each case, it was found that $M_nX_n^+$ ($n = 3$, 6, and 13) clusters had incremental atomization energies that were significantly larger than their immediate neighbors, in agreement with the larger than expected size (in terms of the log-normal plot) of the peaks corresponding to these species in the experimental spectra. Moreover, $M_nX_n^+$ ($n = 5$, 7, and 11) clusters were observed in the calculations to have incremental atomization energies that were significantly smaller than their neighbors, also in agreement with the small experimental abundance of these species in the spectra shown in Figure 1. This agreement indicates that the cations observed in the mass spectra were created during the ablation process and not from photoionization of an ablation-produced distribution of neutral clusters.

Electronic Properties. The geometry optimization of the neutral and cationic clusters provides an opportunity to explore the relationship between cluster size and physical properties. Moreover, one is able to use such data to determine whether

TABLE 5: Calculated Kohn−Sham Orbital HOMO−LUMO Gaps, TD-DFT First Excitation Energies, Calculated Vertical Ionization Energies, and Atomization Energies Per Monomer Unit for Selected Cluster Sizes, (n = 2, 5, 10, and 16). Also Included Are the Literature Experimental Values for the Corresponding Bulk Properties: The Band Gap, E_g, the Photoelectric Threshold, Φ, and the Molar Enthalpy of Atomization, ΔH°_{at}

	$n = 2$	$n = 5$	$n = 10$	$n = 16$	experimental bulk[26]
Kohn−Sham HOMO−LUMO Gap (eV)					
Zn_nS_n	2.78	4.59	4.16	4.42	3.60[a]
Zn_nSe_n	2.69	4.33	3.15	3.89	2.73[a]
Cd_nS_n	2.34	3.99	3.25	3.41	2.47[a]
Cd_nSe_n	2.30	3.80	3.05	3.23	1.67[a]
TD-DFT First Excitation Energy (eV)					
Zn_nS_n	1.63	3.56	3.23	3.68	3.60
Zn_nSe_n	1.03	3.33	2.89	3.28	2.73
Cd_nS_n	1.25	2.95	2.52	2.77	2.47
Cd_nSe_n	1.25	2.82	2.36	2.63	1.67
Vertical Ionization Energy (eV)					
Zn_nS_n	8.48	8.57	8.26	8.30	7.50[b]
Zn_nSe_n	8.11	8.11	7.73	7.74	6.82[b]
Cd_nS_n	8.10	8.27	7.90	7.91	7.26[b]
Cd_nSe_n	7.82	7.80	7.49	7.49	6.62[b]
Molar Atomization Energy (kJ/mol)					
Zn_nS_n	304.1	413.7	444.6	463.2	607.0[c]
Zn_nSe_n	261.6	355.5	381.6	396.4	535.7[c]
Cd_nS_n	226.0	334.8	358.2	376.4	542.3[c]
Cd_nSe_n	209.9	305.2	328.1	343.0	498.3[c]

[a] E_g values. [b] Φ values. [c] ΔH°_{at} values.

there are regularities in these properties. Often, an extrapolation of the molecular properties of the clusters is used (as a function of cluster size) to predict bulk experimental quantities. However, in the case of the chalcogenide clusters, there are gross geometry changes as the cluster size increases, and for most clusters, the geometry is not related to the crystalline structure observed in the bulk material. Rather than selectively using data to provide a linear extrapolation, we have chosen to compare relative properties across the series of chalcogenide clusters and provide cluster/bulk comparisons for members of each subset of cluster geometries. HOMO−LUMO gaps were found for each neutral cluster by calculating the difference between the highest occupied and lowest unoccupied Kohn−Sham eigenvalues. The calculated HOMO−LUMO gaps for selected cluster sizes, n = 2 (planar), 5 (nonplanar), 10 (three-dimensional cage), and 16 (high-symmetry cage), are listed in Table 5. All three combinations of metal and chalcogen display the same basic pattern. The neutral monomer and dimer structures have the smallest HOMO−LUMO gaps, after which the gap quickly increases to its maximum value for the pentamer, the last monocyclic structure. The gaps for the three-coordinate, three-dimensional clusters ($n > 5$) are lower and slowly increase with increasing cluster size. Qualitatively, it was observed that the calculated HOMO−LUMO gaps for all values of n follow the same pattern of increase as the experimentally observed band gaps: $Zn_nS_n > Zn_nSe_n > Cd_nS_n > Cd_nSe_n$. The only exception was the HOMO−LUMO gap of $Zn_{10}Se_{10}$, which was smaller than that of $Cd_{10}S_{10}$.

The spectroscopically observed HOMO−LUMO gap of a cluster or molecule only approximately corresponds to its first excitation energy. Therefore, the first excitation energies for each cluster were also calculated in a series of *time-dependent DFT* calculations at the B3LYP level of theory, with the same basis sets used for the optimizations. The excitation energies of the same selected cluster sizes are also given in Table 5. These first excitation energies are qualitatively similar to the HOMO−LUMO gap energies calculated using the Kohn−Sham orbital difference method, but are significantly smaller for each cluster because the excited states are fully relaxed in these optimizations. This is a more accurate procedure for the comparison of cluster energy gaps with the band-gap energies. One observes that the calculated cluster excitation energies more closely resemble the bulk E_g values. These calculated excitation energies follow the same pattern of increase as the experimentally observed band gaps: $Zn_nS_n > Zn_nSe_n > Cd_nS_n > Cd_nSe_n$. For these calculations, the single exception was the excitation energy of Zn_2Se_2, which had the smallest excitation energy among all of the dimers studied.

The vertical ionization energy of each cluster was calculated by taking the difference between the total energy of the ground-state neutral cluster and the positive ion at the optimized neutral-cluster geometry; see Table 5. For each cluster size, the calculated vertical ionization energies were in the order $Zn_nS_n > Cd_nS_n > Zn_nSe_n > Cd_nSe_n$, which is identical to the order of the experimental photoelectric thresholds, Φ.[26] There were three exceptions to this trend, however: the vertical ionization energies of ZnSe, Zn_2Se_2, and Zn_7Se_7 were calculated to be slightly higher than those of CdS, Cd_2S_2, and Cd_7S_7, respectively. However, the energy differences were very small.

Cluster atomization energies were also calculated per mole of monomer units for each cluster. The calculated atomization energy data for the selected species are found in Table 5. The bulk comparison point here is the value of ΔH°_{at}. For all cluster sizes, the calculated molar atomization energies proceed in the order: $Zn_nS_n > Zn_nSe_n > Cd_nS_n > Cd_nSe_n$. However, the experimental order of the ΔH°_{at} values is: $Zn_nS_n > Cd_nS_n > Zn_nSe_n > Cd_nSe_n$, which is in disagreement with the theoretical prediction. It should be noted, however, that the computed atomization energies of Cd_nS_n and Zn_nSe_n differ very little in all cases.

Summary

Metal chalcogenide nanoclusters were generated by laser ablation of zinc selenide, cadmium sulfide, and cadmium selenide in a time-of-flight mass spectrometer. The mass spectra indicated a common trend, in which clusters with $n = 6$ and 13 were ultrastable. In a parallel study, the geometries and energies of neutral and positively charged M_nX_n clusters up to $n = 16$ were obtained computationally. Small neutral and positive clusters ($n < 5$) have planar geometries, whereas neutral three-dimensional clusters have the geometry predicted by Euler's theorem for closed-cage polyhedra with all atoms in a three-coordinated state. Cationic three-dimensional clusters, on the other hand, have cage structures with a pair of two-coordinated atoms, unless separation of adjacent four-membered rings is not necessary for stability. With increasing cluster size, the molar atomization energies and ionization energies of the neutral clusters were shown to trend toward the qualitative ranking of corresponding bulk parameters: the approximate molar enthalpies of atomization and photoelectric thresholds. In addition, the HOMO−LUMO gaps were calculated using Kohn−Sham one-electron orbital energy differences as well as TD-DFT first-excitation energy calculations and, in both cases, are shown to trend to the qualitative ranking of the bulk band-gap energies. The relative stability of the positive stoichiometric clusters expressed in terms of the incremental atomization energy vs the number of clustering monomer units provides a thermodynamic explanation for the relative stability observed in the laser ablation formation process for d^{10} metal chalcogenide clusters. These results allow one to speculate on the nucleation/growth process. The mass spectrometric and DFT results are consistent

with nucleation modeling results.[26] Clusters are seeded by ions, which polarize nearby atoms in the ablation plasma plume. These atoms become the building material for cluster growth, which is terminated by electron−cation collisions.

References and Notes

(1) Mauch, R. H. *Appl. Surf. Sci.* **1996**, 589.
(2) Ndukwe, I. C. *Sol. Energy Mater. Sol. Cells* **1996**, *40*, 123.
(3) Leskela, M. *J. Alloys Compd.* **1998**, *275*−*277*, 702.
(4) Shi, Y.; Yu, Z.; Zhang, N.; Gao, Z.; Kong, F.; Zhu, Q. *J. Chin. Chem Soc.* **1995**, *42*, 455.
(5) Martin, T. P. *Phys. Rep* **1996**, *273*, 199.
(6) Burnin, A.; BelBruno, J. J. *Chem. Phys. Lett.* **2002**, *362*, 341.
(7) Kukreja, L. M.; Rohlfing, A.; Misra, P.; Hillenkamp, F.; Dreisewerd, K. *Appl. Phys. A: Mater. Sci. Process.* **2004**, *78*, 641.
(8) Matxain, J. M. *Small Clusters of II*−*VI Materials*; Universidad del Pais Vasco: Spain, 2002.
(9) Ziemann, P. J.; Castleman, A. W. J. *Phys. Rev. B: Condens. Matter Mater. Phys.* **1992**, *46*, 13480.
(10) Matxain, J. M.; Fowler, J. E.; Ugalde, J. M. *Phys. Rev. A: At., Mol., Opt. Phys.* **2000**, *61*, 053201.
(11) Burnin, A.; Sanville, E.; BelBruno, J. J. *J. Phys. Chem. A* **2005**, *109*, 5026.
(12) Spano, E.; Hamad, S.; Catlow, C. R. A. *J. Phys. Chem. B* **2003**, *107*, 10337.
(13) Spano, E.; Hamad, S.; Catlow, C. R. A. *Chem. Commun.* **2004**, *7*, 64.
(14) Woodley, S. M.; Sokol, A. A.; Catlow, C. R. A. *Z. Anorg. Allg. Chem.* **2004**, *630*, 2343.
(15) Kasuya, A. S. R.; Barnakov, Y. A.; Dmitruk, I. M.; Nirasawa, T.; Romanyuk, V. A.; Kumar, V.; Mamykin, S. V.; Tohji, K.; Jeyadevan, B.; Shinoda, K.; Kudo, T.; Terasaki, O.; Liu, Z.; Belosludov, R. V.; Sundararajan, V.; Kawazoe, Y. *Nat. Mater.* **2004**, *3*, 99.
(16) Matxain, J. M.; Mercero, J. M.; Fowler, J. E.; Ugalde, J. M. *J. Phys. Chem. A* **2004**, *108*, 10502.
(17) Deglmann, P.; Ahlrichs, R.; Tsereteli, K. *J. Chem. Phys.* **2002**, *116*, 1585.
(18) Troparevsky, M. C.; Chelikowsky, J. R. *J. Chem. Phys.* **2001**, *114*, 943.
(19) Kohn, W.; Sham, L. J. *Phys. Rev.* **1965**, *140*, A113.
(20) Lee, C.; Yang, W.; Parr, R. G. *Phys. Rev. B: Condens. Matter Mater. Phys.* **1998**, *37*, 785.
(21) Straatsma, T. P.; Apra, E.; Windus, T. L.; Dupuis, M.; Bylaska, E. J.; Jong, W. d.; Hirata, S.; Smith, D. M. A.; Hackler, M. T.; Pollack, L.; Harrison, R. J.; Nieplocha, J.; Tipparaju, V.; Krishnan, M.; Brown, E.; Cisneros, G.; Fann, G. I.; Fruchtl, H.; Garza, J.; Hirao, K.; Kendall, R.; Nichols, J. A.; Tsemekhman, K.; Valiev, M.; Wolinski, K.; Anchell, J.; Bernholdt, D.; Borowski, P.; Clark, T.; Clerc, D.; Dachsel, H.; Deegan, M.; Dyall, K.; Elwood, D.; Glendening, E.; Gutowski, M.; Hess, A.; Jaffe, J.; Johnson, B.; Ju, J.; Kobayashi, R.; Kutteh, R.; Lin, Z.; Littlefield, R.; Long, X.; Meng, B.; Nakajima, T.; Niu, S.; Rosing, M.; Sandrone, G.; Stave, M.; Taylor, H.; Thomas, G.; Lenthe, J. v.; Wong, A.; Zhang, Z. *NWChem 4.5, A Computational Chemistry Package for Parallel Computers*;, version 4.5; Pacific Northwest National Laboratory: Richland, WA, 2003.
(22) Becke, A. D. *J. Chem. Phys.* **1993**, *98*, 5648.
(23) Stevens, W. J.; Krauss, M.; Basch, H.; Jasien, P. G. *Can. J.Chem.* **1990**, *70*, 612.
(24) Holden, E. Atomic Masses and Abundancies. In *CRC Handbook of Chemistry and Physics*; David, R. L., Ed.; CRC Press: Boca Radon, FL, 2003; pp 1−15.
(25) Matxain, J. M.; Mercero, J. M.; Fowler, J. E.; Ugalde, J. M. *Phys. Rev. A: At., Mol., Opt. Phys.* **2001**, *64*, 053201.
(26) Swank, R. K. *Phys. Rev.* **1967**, *153*, 844.